Original Research

D. P. Jansik*
D. Wildenschild
N. D. Rosenberg

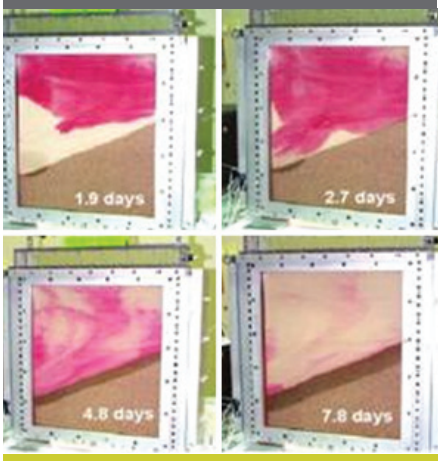

Predicting capillary barrier breach is important for waste containment systems. The results of two benchtop capillary barrier experiments demonstrate the importance of sediment surface roughness and water film flow on capillary barrier effectiveness and show that consideration of dry regime flow processes is essential at low saturations.

D.P. Jansik and D. Wildenschild, School of Chemical, Biological and Environmental Engineering, Oregon State Univ., 102 Gleeson Hall, Corvallis, OR 97331; N.D. Rosenberg, Lawrence Livermore National Lab., Livermore, CA 94551; and D.P. Jansik, Energy and Environment Directorate, Pacific Northwest National Lab., Richland, WA 99352. *Corresponding author (danielle.jansik@pnnl.gov).

Vadose Zone J. 10:1–12
doi:10.2136/vzj2010.0128
Received 26 Oct. 2010.
Posted online 31 Aug. 2011.

Flow Processes in the Dry Regime: The Effect on Capillary Barrier Performance

Engineered capillary barriers typically consist of two layers of granular materials designed so that the contrast in material hydraulic properties and sloping interface retain infiltrating water in the upper layer. We conducted two benchtop capillary barrier experiments, followed by interpretation and numerical modeling. The hydraulic parameters for two coarse materials were measured using standard methods, and we found that the materials had similar hydraulic properties despite being morphologically different (round vs. angular). The round sand provided a better functioning capillary barrier than the angular sand, but neither experiment could be characterized as a perfectly working capillary barrier. In both cases, >93% of the infiltrating water was successfully diverted from the lower layer; however, infiltration into the underlying layer was observed in both systems. Based on this work, we believe that noncontinuum processes such as vapor diffusion and film flow contribute to the observed phenomena and are important aspects to consider with respect to capillary barrier design as well as dry vadose zone processes in general. Using a theoretical film flow equation that incorporates the surface geometry of the porous material, we found that infiltration into the coarse underlying sand layer appeared to be dominated by water film flow. The NUFT (Nonisothermal Unsaturated–Saturated Flow and Transport) model was used for qualitative comparison simulations. We were able to reproduce the barrier breach observed in the experiments using targeted parameter adjustment, by which pseudo-film flow was successfully simulated.

Abbreviations: BET, Brunauer–Emmett–Teller.

Computer simulation models have become essential tools for estimating the physical processes associated with the near-surface environment in almost any scientific or engineering effort involving water resources. The reliable application of computer models depends, however, on the acquisition of representative soil physical properties and accurate representation of the key physical processes. It is common practice to assume that the estimated van Genuchten (1980) or Brooks and Corey (1964) parameters adequately represent the hydraulic properties of the material. Nevertheless, material properties, such as grain morphology and surface roughness, can have a significant effect on the flow and transport behavior in porous media (Tokunaga and Wan, 1997; Tuller et al., 1999).

Both water film flow and vapor diffusion can affect fluid flow in the dry regime; however, they are typically neglected because in most cases their impact is negligible. Under some circumstances, these dry regime flow processes can dramatically alter the system behavior. Nimmo (1991) and Rossi and Nimmo (1994) highlighted assumptions in water retention models that result in unrealistic predictions at low saturations and have extended soil water retention curves to the dry regime. Studies conducted by Hu et al. (2004) examined the impact of water content and thin water films on the movement of a solute through crushed tuff and found solute mobility to be a function of water film thickness and continuity; the presence of water films altered the rate of diffusion within the system and the interconnectedness of the pore space. Recent studies conducted by Aminzadeh and DiCarlo (2010) confirmed that at low infiltration velocities, pore-scale physics controls the infiltration front.

Film flow and vapor diffusion contributions manifest themselves in a similar manner, following what is known as a Washburn relationship where the infiltrated distance is proportional to the square root of time (Bico et al., 2001), and are therefore difficult to decouple.

In this study, we investigated the impact of grain morphology and surface roughness on the prediction of capillary barrier system efficiency, highlighting qualitative differences

in predictive modeling and dry regime flow processes. Standard laboratory measurements of hydraulic properties were measured for two different underlying coarse sands (angular and round) for two capillary barrier experiments. Although van Genuchten parameters fitted to measured capillary pressure–saturation curves indicated that the two materials were hydraulically similar, they behaved differently under experimental conditions when used as a capillary barrier material. In both experiments, >93% of the infiltrating water was successfully diverted from the lower layer; however, consistent infiltration into the underlying layer was observed in both systems. We believe that differences in the experimental results were due to the different surface morphologies of the two coarse materials. In parallel capillary barrier experiments, and using the same angular sand, Tidwell et al. (2003) observed similar breakthrough into the coarse material. The fluid breakthrough was attributed to water film flow or vapor transport.

The present work was focused on resolving which mechanism, film flow or vapor diffusion, is the dominant driver in the experimental system. Using a theoretical relationship developed by Hay et al. (2008) relating surface roughness to infiltration velocity and by quantifying the theoretical vapor flux, we found that the primary mechanism for capillary barrier breach was probably film flow.

When omitting dry regime processes such as (i) film flow and (ii) vapor diffusion, we were unable to predict the water flow observed in the capillary barrier system with the numerical model. Once film flow and vapor diffusion were included in the analyses, however, via model parameter adjustment that simulated flow under very dry conditions, we could reproduce the observed behavior. The relative significance of the film flow component was found to be highly dependent on the surface roughness, with film infiltration velocities increasing with surface roughness as well as wettability.

This work was initially motivated by the need to enhance understanding of engineered capillary barriers constructed from backfill material. Capillary barriers were considered in the preliminary design stage for a potential high-level nuclear waste site. These barriers were considered to be a high-level waste containment system in which a capillary barrier would be established between fine- and coarse-grained materials. Capillary barrier systems are widely applied at landfills and as mine tailing covers. The concepts discussed here are not limited to the conditions associated with a capillary barrier; they apply to many aspects of modeling unsaturated flow and transport in porous media in a dry regime.

Our capillary barrier experiments and qualitative model simulations also provide a good example of potential discrepancies between ideal models and complex experimental systems in a dry regime.

Film Flow

Film flow in unsaturated porous media has been described in many studies (Tokunaga 1997; Tokunaga et al., 2000). Tuller et al. (1999) and Tuller and Or (2001) pointed out that many models neglect film flow by assuming that flow occurs only in full capillaries. Thus, the pressure potential is attributed solely to capillary forces, while other adsorptive surface forces are ignored. This simplified model usually provides satisfactory results for intermediate and highly saturated media but tends to fail at very low saturation (Nimmo et al., 1994).

Tuller et al. (1999, Fig. 1) showed that pore space geometry (the pore shape and angularity of grains) has a marked influence on imbibition and drainage processes. During imbibition, the liquid–vapor interface grows within corners of angular pores with increasing potential (or capillary pressure) to the point of snap off, whereas the round pores go from being empty to being full without the intermediate steps that occur in angular pores. Increases in capillary pressure result in decreasing amounts of liquid in the corners (Tuller et al., 1999).

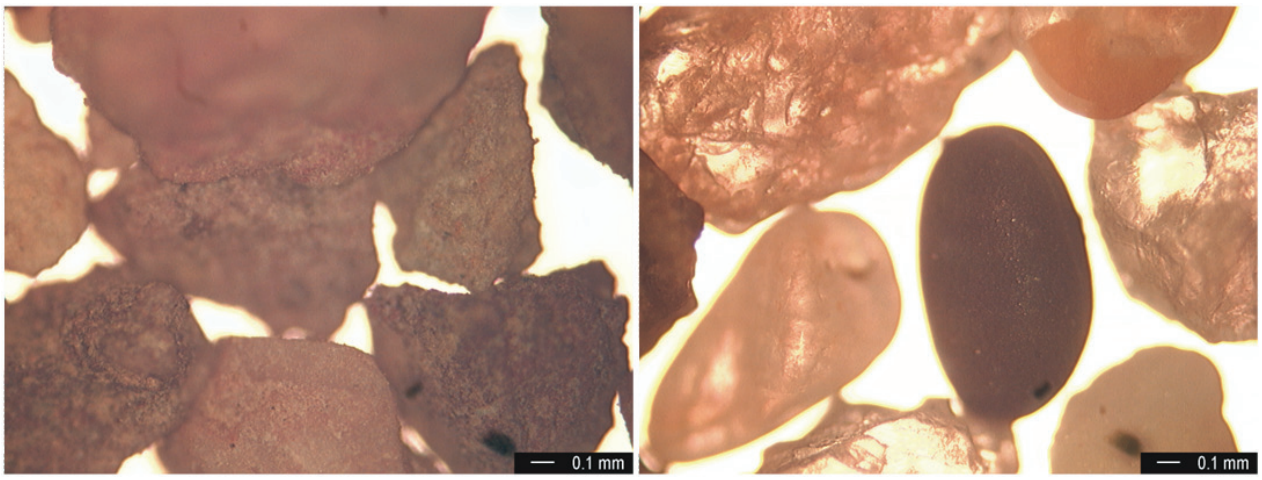

Fig. 1. Light microscopy images of angular sand (left) and round sand (right).

The impact of surface roughness on wettability and contact angle was first conceptualized by Wenzel (1936). Since then, extensive research has been conducted to quantify the effect of roughness on wetting and water film flow (Bico et al., 2001, 2002; Quéré and Bico, 2003; Martines et al., 2005; Hay et al., 2008). Hay et al. (2008) coupled surface geometries with the movement of water films to produce a conceptual model providing a pseudo-sorptivity (or diffusion) term. From this equation, the water film infiltration velocity can be determined using the liquid–surface contact angle, surface tension, viscosity, material surface geometry, and capillary pressure at the point of origin. We used the theoretical expression of Hay et al. (2008) to determine the relative contribution of film flow in our experiments.

Vapor Diffusion

DiCarlo et al. (1999) suggested vapor pressure gradients as a mechanism for enhanced movement of liquid and as an explanation for differences in lateral spreading of moisture fingers observed in experiments. The vapor diffusion approach was based on the conservative assumption that the unsaturated hydraulic conductivity contribution to the sum of liquid and vapor transport (DiCarlo et al., 1999, Eq. [2]) is extremely small at very low fluid saturations. DiCarlo et al. (1999) also assumed that the vapor condensed to liquid behind the vapor front even in the absence of a temperature gradient. The latter assumption has been supported by many studies showing that under equilibrium conditions, vapor will condense, i.e., adsorb to porous media, even though the porous medium has the same temperature as the vapor. Parker (1986) explained that when a dry hydrophilic porous medium is placed in an atmosphere containing water vapor, isothermal water adsorption will increase with increasing vapor pressure until the pore space becomes fluid filled. Similarly, Kutilek and Nielsen (1994) suggested that the nature of soil water adsorption through hygroscopicity is completely different from the simple process of vapor condensation to its liquid phase. Adsorption phenomena are generally classified as being either physical (based on electrostatic and van der Waals attraction forces between a solid surface and water molecules) or chemical (based on rearrangement of electrons and consequent formation of strong chemical bonds) (Parker, 1986; Nitao and Bear, 1996). The adsorbed water layers coating the solid grains grow into films, and eventually adsorbed films in adjacent pore spaces will coalesce and form a continuous liquid phase in the pore. This process is generally referred to as *capillary condensation* (Derjaguin and Churaf, 1976; Tuller et al., 1999). According to Easton and Machin (2000), there is no well-defined limit to the amount of vapor that can be absorbed to a wetting fluid; however, Tokunaga and Wan (2001) suggested that water films range in thickness from tens of nanometers to ~1 μm. The adsorption of water vapor is aided by the vapor pressure deficiency that exists across a concave surface (air–water meniscus in a pore) compared with the vapor pressure across a free, flat water surface (Bear, 1988).

In contrast, Conca (1990) found that four size fractions of tuff gravel remained dry after equilibrating for 70 d at nearly 100% relative humidity. At the conclusion of the experiment, only a 2.7% increase in intergranular water content was observed, indicating that the relative importance of vapor diffusion for water infiltration may be minimal.

Vapor diffusion enhancement could contribute to the observed infiltration into an underlying layer but is generally considered to occur primarily where a temperature gradient is present (Cass et al., 1984; Wildenschild and Roberts, 2001). Ho and Webb (1998), however, reported both experimental and numerical modeling evidence of the enhancement of vapor diffusion in the absence of a thermal gradient. According to their study, the vapor density gradient, which drives the enhancement, can be established without the influence of a thermal gradient, for instance due to the presence of liquid islands. In either case, enhancement across liquid bridges in a coarse material is possible but a fairly unlikely explanation for our system because capillary action would be a more efficient transport mechanism at the saturation at which liquid islands develop.

Thus the question remains, what is the relative impact of vapor diffusion and water film infiltration in unsaturated systems? We believe that it is likely that both processes are occurring simultaneously. Our experiments were targeted at understanding the importance of dry regime flow processes in a working capillary barrier system.

Experimental Design

Materials

We conducted two experiments using commercially available Overton fine silica sand (no. 50–70 sieve) as the fine material and either angular sand (no. 8–20 sieve), consisting of crushed volcanic tuff, or round quartz sand (no. 2–16 sieve) as the coarse layer. The two experiments are referred to as Exp. 1 and 2, respectively. The coarse material for Exp. 1 was selected for its utility as a possible future backfill and was obtained from a supplier in Nye County, Nevada. For Exp. 2, sand with a similar grain size distribution was used, but we chose a material with a lower surface area and more rounded grains. The fine-grained material was selected such that it would not filter into the coarse-grained material under dry conditions. Additional details about material properties are provided in Table 1.

Surface Area Analysis

Specific surface areas for the two coarse sands were measured using the Brunauer–Emmett–Teller (BET) technique (Brunauer et al., 1938). Both the total surface area and the micropore area were measured in duplicate and the results are listed (as averages of the measurements) in Table 1. The angular sand had 10 times more total specific surface area than the round sand, and the angular sand micropore area alone matches the total surface area of the round sand.

Table 1. Material properties of the sands used in this study.

Parameter	Angular sand	Round sand	Overton fine sand
Grain size distribution, mm			
0.053	0.47	–	2.08
0.1	0.77	–	55.58
0.25	1.27	0.06	39.24
0.42	–	0.54	–
0.5	32.7	–	3.06
0.575	–	2.23	–
1.0	64.83	62.73	0
1.41	–	34.19	–
2.0	2	0.21	0
d_{50}†	0.58	0.87	0.091
d_{60}/d_{10}‡	3.42	1.56	2.07
Surface area, $m^2\ g^{-1}$			
Total	2.908	0.227	
Micropore	0.230	0.040	

† Median particle size.
‡ Uniformity coefficient.

Figure 1 shows microscopic photos of the two materials; the difference between the two is quite apparent. The round sand (Exp. 2) is a uniform quartz sand while the angular sand (Exp. 1) is a crushed tuff consisting of angular grains containing various minerals and exhibiting intragranular porosity, differences that result in very different pore shapes.

Hydraulic Parameters

The hydraulic characteristics of the materials were measured separately in smaller sample holders. The capillary pressure–saturation characteristics were measured using a quasi-static approach (Wildenschild et al., 1997) in a smaller (Tempe cell type) pressure cell (7.6-cm diameter, 3.5 cm long). Saturated hydraulic conductivity was measured in a column (2.5-cm diameter, 28 cm long) using the constant-head technique (e.g., Klute, 1986), with three different hydraulic gradients for each sample. The unsaturated hydraulic conductivity was estimated from the capillary pressure–saturation data. The resulting capillary pressure–saturation and unsaturated hydraulic conductivity curves for all materials used are illustrated in Fig. 2 and 3. A nonlinear least-squares optimization routine (RETC version 6.0, U.S. Salinity Lab., Riverside, CA) was used to fit van Genuchten (1980) parameters (listed in Table 2) to the data. The two coarse materials had similar hydraulic properties except for a noticeable difference in residual saturation (Table 2) and a small difference in air-entry pressure; compared with the fine layer (Overton sand), they are very similar.

Laboratory Setup: Capillary Barrier System

The capillary barrier experiments were performed in a benchtop aluminum box (60.5 by 56.0 by 10 cm) with a Pyrex window on one side allowing easy visualization of flow patterns (see Fig. 4). Two 50-kPa tensiometers were installed from the back side of the box (marked as squares in Fig. 4). The tensiometers consisted of porous ceramic cups glued onto the back side of the box that, via testing, were confirmed to have an air-entry value of >250 cm

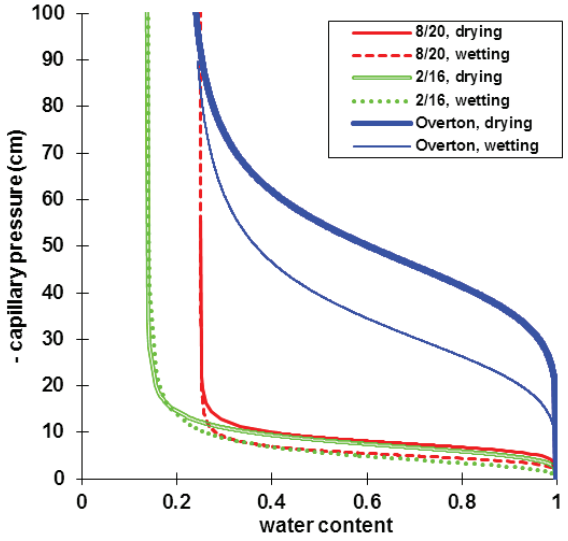

Fig. 2. Capillary pressure–saturation curve for the angular sand (8/20), round sand (2/16), and Overton sand.

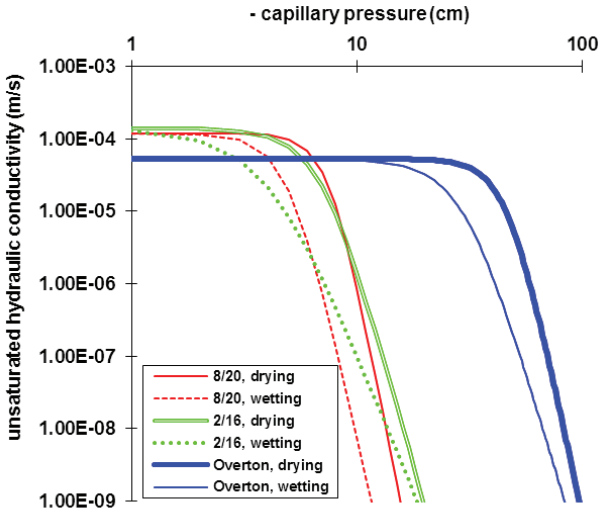

Fig. 3. Estimated capillary pressure–unsaturated hydraulic conductivity curve for the angular sand (8/20), round sand (2/16), and Overton sand.

Table 2. Material hydraulic properties, including fitting parameters α and n, saturated and residual volumetric water contents (θ_s and θ_r, respectively), and saturated hydraulic conductivity (K_s) of the sands used in this study.

Sand	α	n	θ_s	θ_r	R^2	K_s
	cm^{-1}					$m\ s^{-1}$
Round, drying	0.139	4.69	0.37	0.05	0.997	
Round, wetting	0.231	3.25	0.37	0.05	0.997	1.4×10^{-4}
Angular, drying	0.130	6.65	0.48	0.12	0.996	
Angular, wetting	0.197	5.64	0.48	0.12	0.998	1.2×10^{-4}
Overton, drying	0.021	6.06	0.37	0.08	0.999	
Overton, wetting	0.032	4.39	0.37	0.08	0.999	5.3×10^{-5}

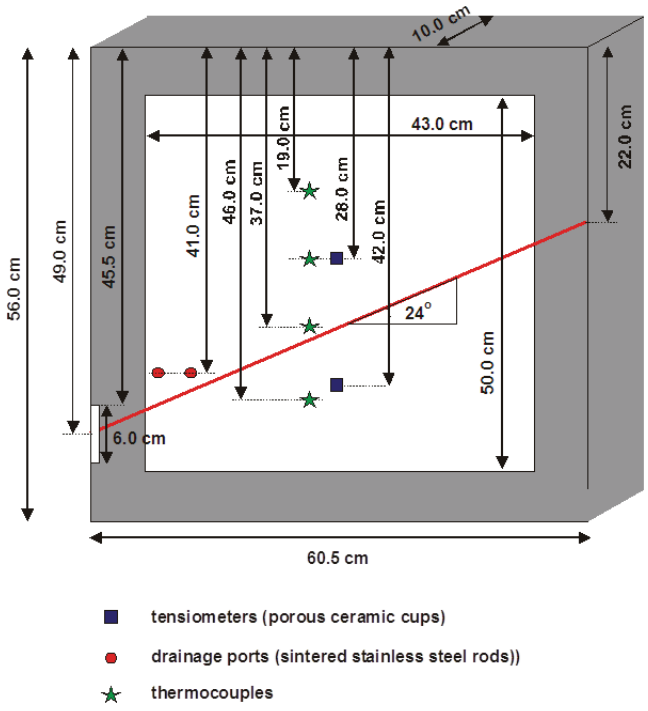

Fig. 4. Experimental setup showing locations of tensiometers, drainage ports, and thermocouples. The white rectangle on the lower left is a secondary porous plate used for checking pressure measurements.

before use. Drainage out of the box was achieved by the use of two stainless steel sintered rods installed on the back side of the box immediately above the fine–coarse interface (circles in Fig. 4). These drains had relatively low air-entry values (<70 cm) and, as a result, were highly permeable such that water flow out of the box was not inhibited. The rods were connected to water-filled tubing, providing negative pressure to facilitate drainage under less than fully saturated conditions. Temperature variations during the experiments were measured with four thermocouples (1.02-mm diameter) placed in the box as shown in Fig. 4 (stars).

Before the materials were packed, the box was tilted to a 24° angle so that the fine–coarse interface was horizontal during packing. The sandy materials were packed loosely in the box to simulate the emplacement of porous material using a conveyor belt, such as would potentially be used at a large-scale nuclear waste repository. As expected, the porosities of the materials varied slightly between the loose packing of the experimental box and the packing in the smaller pressure cells that were used for the hydraulic property measurements. The material packed in the pressure cells typically had a lower porosity than the experimental boxes. We assumed that the

Table 3. Flow rates and boundary conditions for the experiments.

Parameter	Exp. 1: Overton over angular sand	Exp. 2: Overton over round sand
Avg. pump rate, mL h^{-1}	29.8	29.3
Avg. pump rate, m s^{-1}	1.37×10^{-7}	1.35×10^{-7}
Avg. outflow rate, mL h^{-1}	27.8 ± 0.8	29.2 ± 1.3
Avg. fine layer pressure, cm	-32.9 ± 2.8	-35.7 ± 2.8
Avg. drain pressure, cm	-43.2 ± 1.5	-46.3 ± 2.1

largest source of error in hydraulic parameters between the two systems was associated with calculation of the porosity due to minor inaccuracies in the material weights (loss during packing, etc.) and difficulty in precisely estimating the geometric boundaries of the individual layers. Table 3 lists relevant information from the experiment. An irrigation device was placed on top of the box to provide uniformly distributed infiltration over the entire surface area of the top of the box. A water-filled reservoir with 64 drippers (0.25-mm i.d. tubing and finger-tight fittings) was connected to a diaphragm pump. The pump rates were tested before and after each experiment and are listed in Table 3. At the end of the experiment, successive layers were carefully removed and samples (approximately 25 mL) were collected at increasing depth into the coarse layer. The samples were weighed and placed in a 105°C oven overnight and subsequently weighed again to determine the water saturation.

Results

Capillary Barrier Experiments

Irrigation and outflow rates for the two experiments are shown in Fig. 5. Each experiment had an initial increase in the outflow rate until steady-state flow conditions were established. Irrigation and outflow rates, and the average and standard deviations of the outflow rates, are also listed in Table 3. The average rate of infiltration into the underlying coarse layer (estimated as the irrigation pump rate minus the measured drainage rate) for Exp. 1

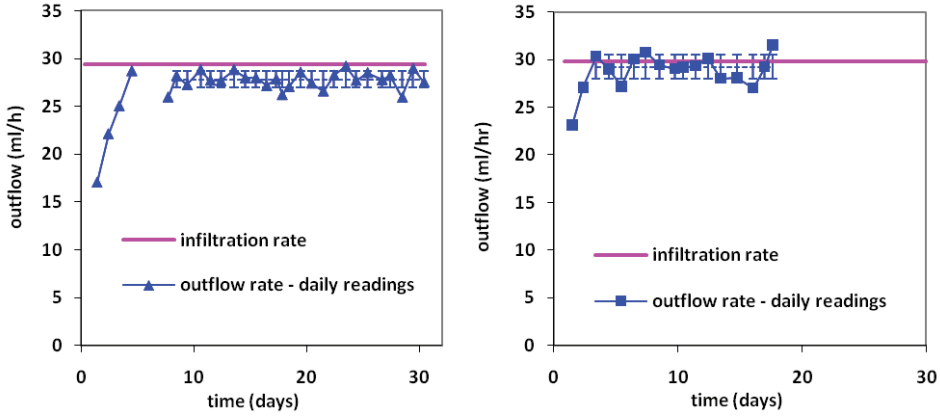

Fig. 5. Water balance for Exp. 1 (Overton over angular sand) (left), and Exp. 2 (Overton over round sand) (right). Infiltration rate is the rate at which water (irrigation) was added to the top of the box. Error bars indicate measurement error.

was 2.0 mL h^{-1} or 9.2×10^{-9} m s^{-1}, and for Exp. 2 only 0.1 mL h^{-1} (which is less than the standard error in the outflow rate) or 4.6×10^{-10} m s^{-1}. These numbers show that (assuming minimal or at least similar evaporation and other losses), the infiltration into the angular sand was 20 times greater than the infiltration into the round sand. As seen in Fig. 5, some water was retained in the coarse layer in Exp. 1 (Overton sand over angular sand); the outflow rate was lower (by more than one standard deviation) than the average irrigation rate. The drains diverted an average of 93.3% of the infiltrating water, which means that, on average, the infiltration front moved at a rate of 6.7% of the applied irrigation rate. This compares reasonably to the approximately 10 to 20% of the applied rate that Tidwell et al. (2003) found using the same angular sand. In Exp. 2, using the round sand as the coarse material, the outflow rate was within a standard deviation of the infiltration rate, and the amount of water being withheld in the coarse layer was within measurement error. The amount of water diverted in this case was 99.7%.

The drain pressure and tensiometer readings for the two experiments were monitored for the duration of the experiments. The air-entry value of the lower tensiometer (placed in the initially dry coarse material) was exceeded during the extended wetting procedure for both experiments and thus no pressure readings are available for this layer. After an initial adjustment period, the drain pressure was almost constant throughout the first experiment (-43.2 ± 1.5 cm); the capillary pressure measured at the upper tensiometer (in the fine material) varied slightly more (-32.9 ± 2.8 cm). The more notable fluctuations in capillary pressure in the experiments were closely correlated to measured temperature variations in the box (not reported here) and are attributed to the temperature sensitivity of the transducers. In the second experiment, the upper tensiometer was also fairly constant, apart from temperature-induced variations (-35.7 ± 2.8 cm). In this experiment, the average drain pressure was -46.3 ± 2.1 cm, similar to Exp. 1. A ceramic plate (initially intended for drainage) functioned as an additional tensiometer, and the measured capillary pressures were nearly identical to the capillary pressures measured at the upper tensiometer. The fact that practically identical values were measured at both vertical locations indicates that flow had reached steady state and was driven by gravity alone.

To better illustrate the flow patterns in the experiment, a dye tracer (phenol red) was sprinkled on the sand surface, where it dissolved in the irrigation water. In the first experiment, it was added at the beginning of the experiment (initially dry sand); in the second experiment, it was added after 5 d, when the wetting front had already reached the material interface. Phenol red is a very conservative tracer with low adsorption capabilities. To document the infiltration, images were periodically collected during the experiment. A time-lapse series of photographs for Exp. 1 and 2 is shown in Fig. 6. It is evident that, in both experiments, the water moved consistently into the coarse layers and that water infiltrated faster (and farther) into the angular sand than into the round sand. This is in agreement with the amounts of water diverted by the drains for the two experiments: as reported above, 6.7% and 0.3% of the infiltrated water was retained in the coarse layer for the first experiment (angular sand) and second experiment (round sand), respectively. Tidwell et al. (2003) used materials that were identical to our Exp. 1 and reported similar results: the barrier effectively diverted the majority of the infiltrating water, but slow and continuous infiltration into the coarse layer occurred (Tidwell et al, 2003, Fig. 2) almost immediately after the wetting front reached the capillary interface.

From post-experiment water saturation measurements, we determined that the wetting front progressed approximately 14 cm into the angular sand, whereas only a narrow band of approximately 2 cm was wetted in the round sand. By analyzing the photographs of the experimental box taken at regular intervals and scaling the infiltrated distance to a feature of known length in the image, we estimated the infiltrated distances as a function of elapsed time, as illustrated in Fig. 7. The infiltrated distance is plotted as a function of $t^{1/2}$; it is clear that the infiltration follows this relationship almost perfectly.

Dry Regime Experiments

To further explore the observed differences between the capillary barriers consisting of the angular or round sand, alternative physical flow mechanisms must be considered. Two different questions need to be addressed: (i) how do we account for the slow, but constant, wetting of the coarse layer, which happens near the fine–coarse layer interface in both experiments; and (ii) why is there such a large variation in wetting front saturation and depth for the two different coarse materials (despite the fact that they have very similar hydraulic properties)?

We believe that the primary causes of enhanced infiltration in the two systems were flow processes specific to the dry regime. To further explore this hypothesis, supplemental experiments were conducted to examine the relative role of vapor diffusion and film infiltration. Because the dry regime processes were most clearly demonstrated in Exp. 1, the angular sand was used for additional measurements of vapor diffusion.

Vapor Diffusion Experiments

Vapor diffusion onto sand samples was monitored gravimetrically. Ten grams of angular sand was dried at 105°C and placed in a closed container with an open reservoir of water. The relative humidity was monitored using a relative humidity sensor; for the duration of the experiment, the humidity remained near 95%. The change in the mass of the sand sample was monitored for a period of 10 d using an analytical balance accurate to ±0.001 g.

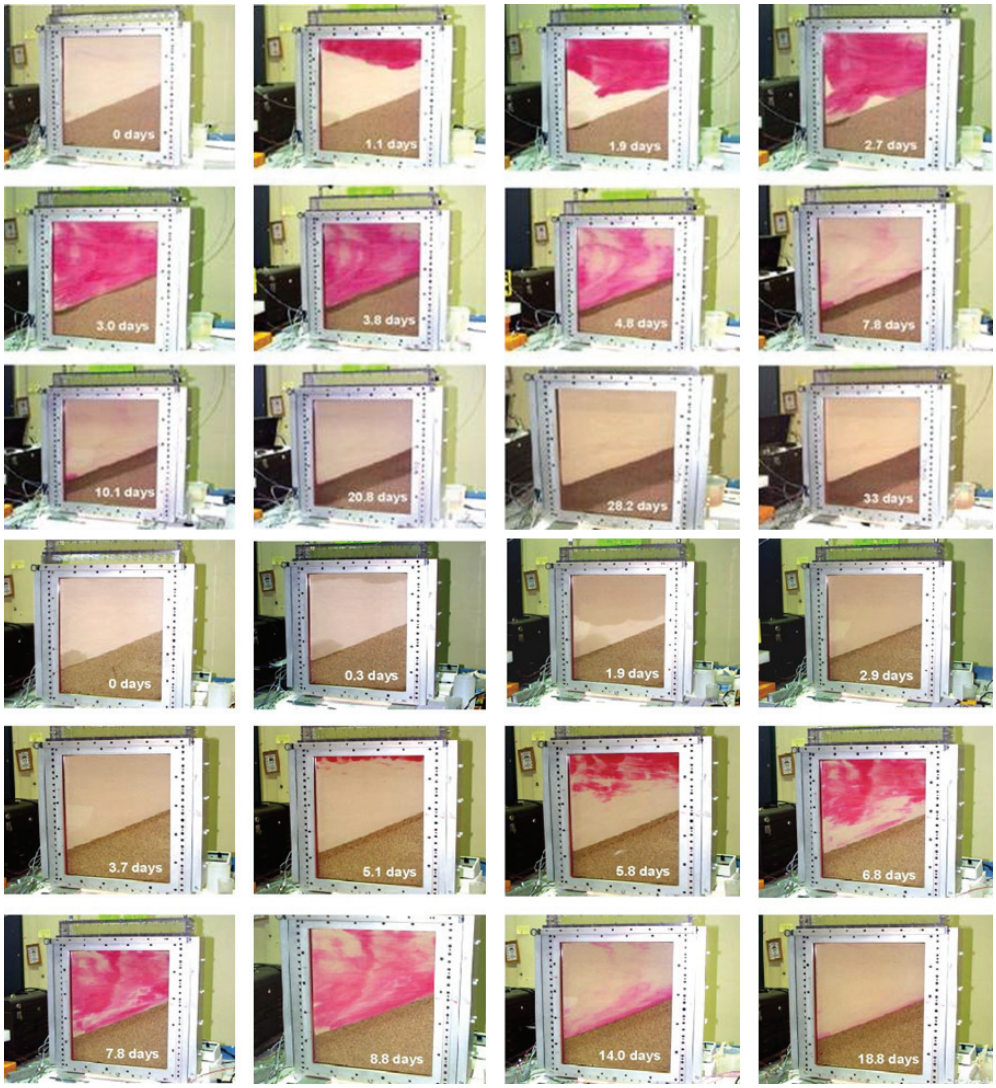

Fig. 6. Dye tracer transport time lapse for Exp. 1 (angular sand) (top) and Exp. 2 (round sand) (bottom).

Material Surface Characterization (in Support of Film Flow)

Surface profiles of the angular and round sand were obtained using a Nanomics Multiview 1000 atomic force microscope system (Nanomics Imaging Ltd., Jerusalem), with a 70-μm scanner in noncontact mode with a noncontact probe. Image analysis using WSxM image processing software (Nanotec Electronica, Madrid) was used to obtain the average amplitude (δ) and wavelength (λ) of material surface features.

Interpretation of Dry Regime Experiments

The dry regime experiments illustrated that vapor diffusion onto sand surfaces in the absence of a gradient was minimal. During a period of 10 d, the mass change in the weight of the sand was within the margin of error of the analytical balance. As mentioned above, similar findings were reported by Conca (1990), who determined the vapor diffusion coefficient for tuff gravel samples to be 10^{-15} m^2 s^{-1} (or 8.6×10^{-7} cm^2 d^{-1}). It should be noted that our experiments were conducted during a relatively short period of

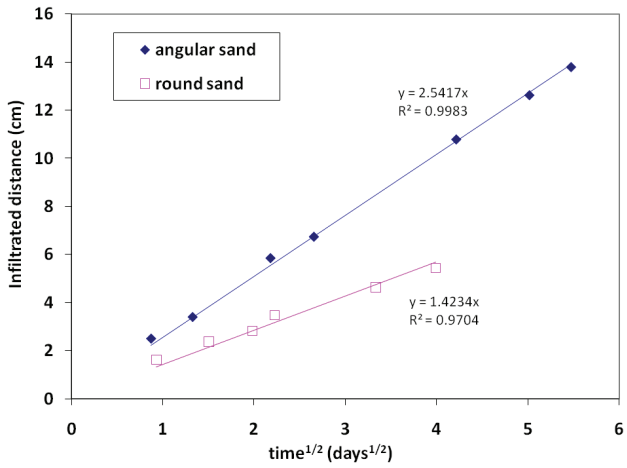

Fig. 7. Infiltration distance vs. the square root of time in Exp. 1, angular sand (closed symbols), and Exp. 2, round sand (open symbols).

time; if repeated for a significantly longer time period, increased weight due to vapor transport may have been observed.

At the saturated fine–coarse material interface, the relative humidity was expected to be near 100%. Because the dry coarse material was overlain by wet fine sand, the relative humidity within the pore space of the coarse sand would equilibrate within hours. Therefore, we postulate that due to the lack of a gradient in the vapor concentration and the low vapor diffusion coefficient, the impact of vapor diffusion on fluid movement in these experiments was minor compared with film flow.

To further probe the potential impact of vapor diffusion on the sustained infiltration into the coarse underlying layer, we also calculated vapor diffusion estimates based on DiCarlo's estimate (DiCarlo et al., 1999, Eq. [9]) and based on a traditional Fickian approach applied to soils (Cass et al., 1984):

$$J_v = -a\alpha D\nabla\rho$$

where J_v is the mass flux density of water vapor (kg m^{-2} s^{-1}), D is the diffusion coefficient of water vapor in air (m^2 s^{-1}), $\nabla\rho$ is the water vapor density gradient (kg m^{-4}), a is the volumetric air-filled porosity (m^3 m^{-3}), and α is a dimensionless tortuosity factor generally assumed to be 0.66 for isothermal flow. The DiCarlo estimate is based on the conservative assumption that the unsaturated hydraulic conductivity contribution to the sum of liquid and vapor transport (DiCarlo et al., 1999, Eq. [2]) is extremely small at very low fluid saturations and that the vapor condenses to liquid behind the vapor front even in the absence of a temperature gradient. This is further supported by Jabro (2009), who found the rate of water vapor gain in larger soil aggregates to be minimal at room temperature. Figure 8 shows the comparison of the DiCarlo and Fickian vapor fluxes with the measured infiltration rates for Exp. 1. The cumulative vertical flux in these figures was calculated based on the saturation measured at the front edge of the wetting front with time, which was 10.8%, and takes into account the ambient relative humidity of 85%. The driving gradient for vapor transport would be the relative difference between the saturated and ambient humidities in the experimental system. The measured vertical flux for the angular sand experiment was approximately 10 times higher than the Fickian estimate and three times higher than the DiCarlo estimate, for a relative humidity of 85%. If the internal relative humidity was closer to 100%, as would be expected for the closed box used in these experiments, the DiCarlo and Fickian estimates would be even lower due to the lack of a driving gradient. It is therefore not possible to explain the observed infiltration into the angular sand based on vapor diffusion based phenomena alone.

To confirm our hypotheses and verify the proposed dominance of film flow in the capillary barrier experiment, we applied an expression for film flow infiltration, based on Wenzel wetting (Hay et al., 2008), to the measured material surface characteristics described above:

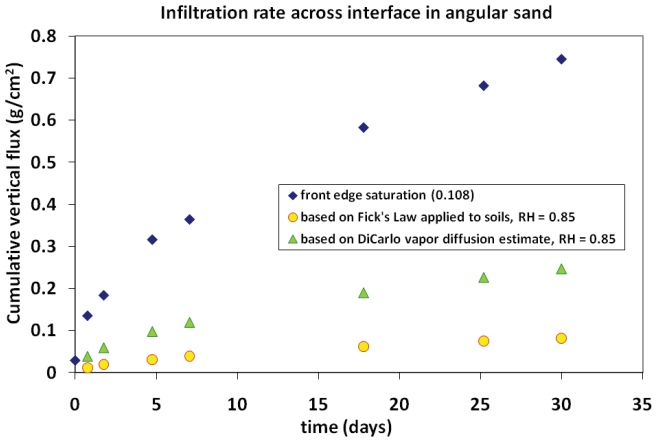

Fig. 8. Infiltration rate into angular sand using Fick's law and DiCarlo estimate calculated using the measured saturation at the front of the wetting front and a relative humidity (RH) of 0.85.

$$x_{h-p} = \left\{\frac{\gamma\delta^2}{4\mu}\left[\frac{(2\delta+\lambda)\cos\theta-\lambda\sin\theta}{\lambda\delta}\right]\right\}^{1/2} t^{1/2} = St^{1/2}$$

Including a negative capillary pressure at the coarse–fine interface, the above equation becomes

$$x_{h-p} = \left\{\frac{\delta^2}{4\mu}\left[-P+\gamma\frac{(2\delta+\lambda)\cos\theta-\lambda\sin\theta}{\lambda\delta}\right]\right\}^{1/2} t^{1/2} = St^{1/2}$$

where x_{h-p} is the infiltration distance (cm), γ is the surface tension (7.2×10^{-2} N m^{-1} for water at 20°C), δ is the average amplitude of the surface features (nm), λ is the average wavelength of the surface features (nm), μ is the kinematic viscosity (1.02×10^{-3} Pa s at 20°C), t is time (s), θ is the contact angle of the water with the material (°), P is the capillary pressure at the coarse–fine interface, and S is the sorptivity (or diffusion) term (m s$^{-1/2}$). Using this relationship and the measured quantities obtained from the atomic force microscopy measurements given in Table 4, we obtained a theoretical sorptivity term of 7.7 cm d$^{-1/2}$ for the angular sand and 5.7 cm d$^{-1/2}$ for the round sand, using a contact angle of 7° for both. Adjusting for tortuosity, the vertical length of travel is one-third the actual travel distance (Dullien, 1992), and the estimated sorptivity terms become 2.63 and 1.90 cm d$^{-1/2}$, which match the

Table 4. Average surface properties of the angular and round sands.

Property	Angular sand	Round sand
	nm	
Amplitude (δ)	3.8	2.5
Wavelength (λ)	50.0	2000.0

angular and round sand experimental values of 2.54 and 1.42 cm $d^{-1/2}$ quite well (Fig. 7).

It should be noted that the sorptivity term varies as a function of the contact angle of the water–sand interface; Fig. 9 illustrates this relationship. In the range of 0 to 15°, however, the calculated sorptivity term varies by only 0.2 cm $d^{-1/2}$.

Numerical Modeling

To further support our experimental findings, we performed comparison simulations using the US1P module of the NUFT (Nonisothermal Unsaturated–Saturated Flow and Transport) model (van Genuchten 1980; Nitao, 1998). This module solves the two-dimensional equations for single-phase unsaturated flow in porous media using Richards' equation. Because of difficulties in matching the measured hydraulic properties (most importantly, the porosity) between the Tempe cell based measurements and those obtained from the experiments, we emphasize the qualitative nature of these results. These simulations are included because they conceptually show how film flow can be simulated using a traditional numerical model, and they also favorably support our interpretation of the experiments. For brevity, we have not included a full parameter listing.

Before performing these comparison simulations, we tested the model against the results reported in Webb (1997) and found that the NUFT simulations were in excellent agreement with those results.

The two-dimensional model simulation domain is shown in Fig. 10. The relationship between saturation, capillary pressure, and hydraulic conductivity is described using the van Genuchten (1980) and Mualem (1976) expressions. The initial condition for the simulations was completely dry sand, and the top boundary and the drain were held at constant head and saturation. The irrigation rate and drain pressure used in the simulations were those measured in the experiments (see Table 3). Simulations for Exp. 1 and 2 were run for a similar length of time as the laboratory experiments (30 and 20 d, respectively).

Because the experimental results indicated that film flow is the dominant cause of the observed behavior, we implemented the use of two parameters in NUFT that we anticipated would result in a pseudo-film-flow situation. To accomplish this, we utilized parameters in the NUFT code that dictate how capillary pressure is implemented for saturations S below residual ($S < S_r$). The NUFT model uses a default setting for the S_j parameter, which determines how capillary pressure is assigned in the absence of data. Adjusting S_j to a lower value implements a higher capillary pressure at the lower saturation end (between 0 and S_r) than used in the default case. This feature in NUFT, and in most unsaturated models where such a feature exists, is not often used because flow properties in this very dry end of the saturation regime are typically not important. We also adjusted the S_r value because this is obviously the parameter

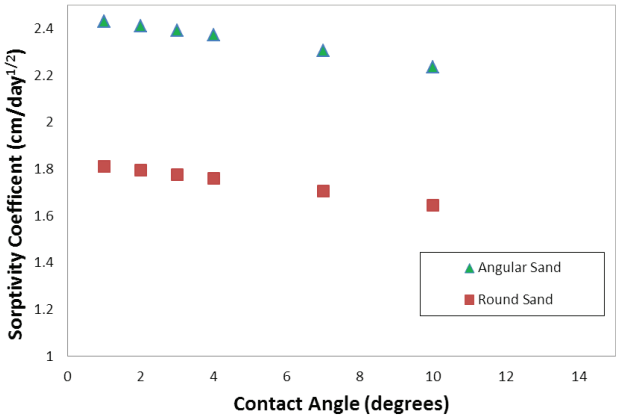

Fig. 9. Sorptivity of infiltrating film as a function of contact angle.

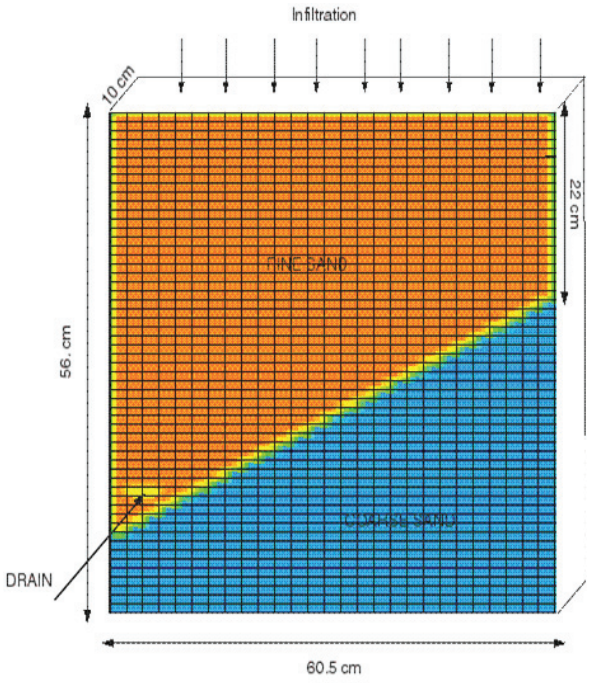

Fig. 10. Experimental domain for the NUFT modeling of a capillary barrier system.

determining at which point flow ceases in the model; by lowering the S_r value, the model allows flow to take place below the measured S_r value, thus effectively simulating film flow. The qualitative comparison resulting from these simulations is discussed below.

Model Results

The parameter adjustments used in the qualitative model comparison are detailed in Table 5. Examples of the resulting simulations are shown in Fig. 11 and 12. The left-hand plots in Fig. 11 and 12 show the simulation results obtained using the baseline parameter set; there is clearly no breach of the barrier with this input parameter set. The S_j parameter was then decreased enough to see small changes in the resulting saturation profile, i.e., a small amount of infiltration across the interface (model results not

shown). To produce this result, the S_j parameter was changed by 11 and 18% for the angular and round sand, respectively; however, despite the barrier now being breached with this modification, the substantial infiltration observed in the experiment was not matched. To further promote film flow, the S_r value, below which the S_j parameter becomes operational, was also lowered, by 22 and 7% for the angular and round sand, respectively. The final S_r value adjustment resulted in saturation profiles similar to those observed at the conclusion of Exp. 1 and 2 (30 d for the angular sand and 20 d for the round sand) (see right-hand images in Fig. 11 and 12). Comparison between the simulation of the angular sand and that of the round sand shows that we captured the major differences in the infiltration patterns between these two systems. We emphasize that no attempt was made to optimize the parameters; the motivation was to qualitatively assess whether a parameter adjustment targeted at film-flow simulation could produce infiltration and saturation patterns similar to those observed in the experiments. This was the case and provides further support for our hypothesis of film flow as the dominant mechanism for infiltration in the dry regime.

Table 5. Summary of NUFT model parameter adjustment.

	S_j†		Residual saturation (S_r)	
Adjustment	Value	Change	Value	Change
		%		%
Exp. 1				
Original parameters	0.2875	–	0.25	–
Adjusted S_j	0.255	11.3	0.25	–
Adjusted S_j and S_r	0.255	11.3	0.195	22.0
Exp. 2				
Original parameters	0.183	–	0.14	–
Adjusted S_j	0.15	18.0	0.14	–
Adjusted S_j and S_r	0.15	18.0	0.13	7.1

† The Sj parameter defines the shape of the capillary pressure curve below Sr.

Discussion

The phenomena observed were probably due to the combined effect of the two processes because water film infiltration and vapor diffusion rarely occur completely separate from each other. In a similar

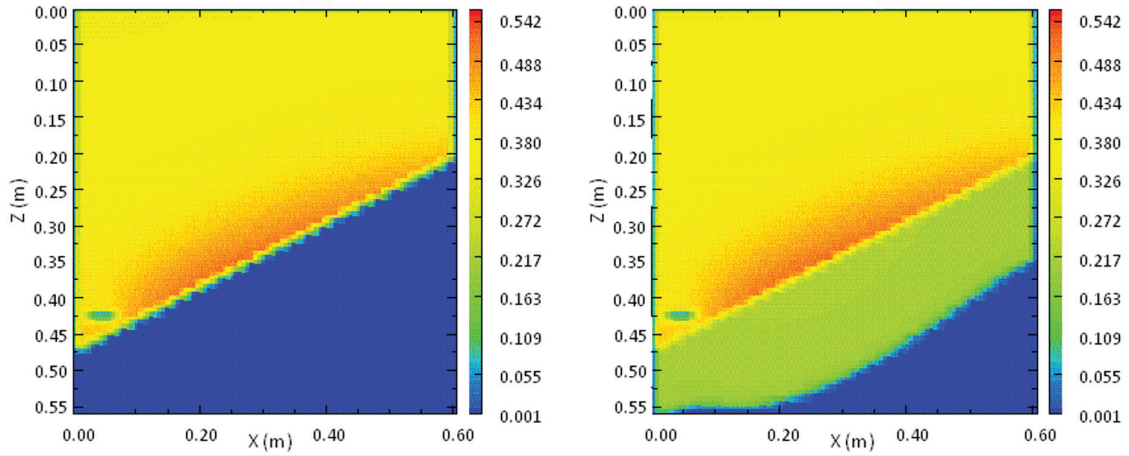

Fig. 11. Simulated saturation fields after 30 d for Exp. 1 (angular sand) using the base hydraulic parameters (left) and using the pseudo-film-flow parameter set (right).

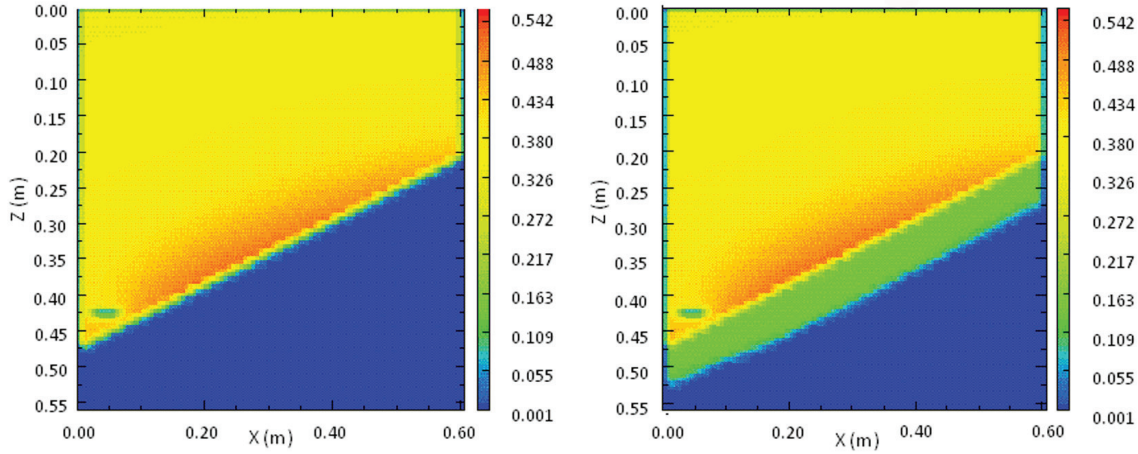

Fig. 12. Simulated saturation fields after 20 d for Exp. 2 (round sand) using the base hydraulic parameters (left) and using the pseudo-film-flow parameter set (right).

experiment, Tidwell et al. (2003) proposed that because blue dye was absent in the infiltrated water (assuming that the large organic molecule was filtered out by films and evaporation), the observed slow but constant infiltration into the dry layer must be caused by the combined action of vapor diffusion and film flow. The rate of infiltration measured by Tidwell et al. (2003) was initially 20%, slowing to 10% after 112 d. These rates are higher than the infiltration observed in the experiments presented here; however, differences may be due to variations in experimental design and boundary conditions.

The interaction of the two processes is schematically illustrated in Fig. 13. Initially, water vapor flows through the sand and some of the vapor adsorbs onto the grains (Fig. 13a and 13b) while the remainder flows or diffuses through the open space between the grains (Tzevelekos et al., 2000). At increasing vapor pressures, water continues to be adsorbed onto the grains in multiple monolayers as long as sufficient water vapor is provided by vapor diffusion for this process to take place (Fig. 13b and 13c). With time, sufficiently thick films may form to facilitate flow (Fig. 13c and 13d). Eventually the films on adjacent grains can coalesce via capillary condensation, initially in the finer pores, resulting in enhanced conductivity and actual capillary action (Fig. 13e and 13f).

The timescales at which we observed water moving through the coarse material, however, indicate that vapor diffusion is not the dominant mechanism. As indicated by Conca (1990), and our own supporting experiment, vapor adsorption is minimal even under conditions of nearly 100% relative humidity. In the experiment of Conca (1990), vapor diffusion and capillary condensation onto similar crushed tuff material accounted for only a 2.4% change in intergranular moisture content.

In contrast, studies conducted by others (Bico et al., 2001, 2002; Quéré, 2002, 2008; Quéré and Bico, 2003; Ishino et al., 2004) have indicated that surface wetting resulting when water films flow over rough materials can occur nearly instantaneously. Martines et al. (2005) and Bico et al. (2001) illustrated that the movement of fluid across a surface of fabricated nanopatterns could be predicted by hemi-wicking theory, where fluid infiltration is a function of the wettability and surface geometry of a material. Using the Hay et al. (2008) expression relating sediment surface geometry to infiltration, we estimated the sorptivity coefficient, which provided a reasonable approximation of the measured infiltration into the underlying layer of the capillary barrier system in Exp. 1 and 2.

Differences in diversion capacity and barrier stability between Exp. 1 and 2 were probably due to the differences in surface properties of the angular and round sands. As illustrated in Fig. 1, by the BET data, and the atomic force microscopy data (Table 4), the surface of the angular sand was significantly rougher than that of the round sand.

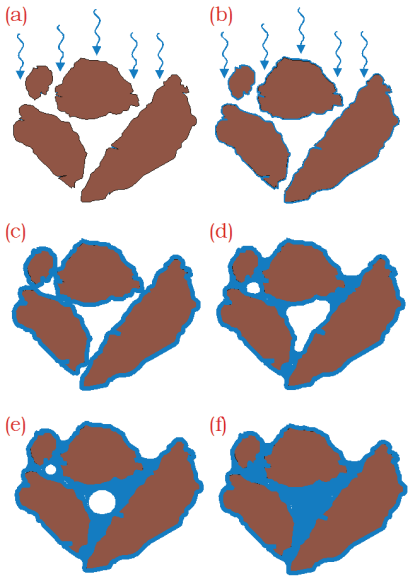

Fig. 13. Hypothesized combined effect of vapor diffusion and film flow on initial infiltration into dry soils.

Conclusions

We conducted two capillary barrier experiments using almost identical initial and boundary conditions but using different underlying (coarse) materials. The coarse materials had very similar hydraulic properties but were morphologically different. The round sand provided a better functioning capillary barrier than the angular sand, but neither of the materials (in combination with the fine Overton sand) provided a perfectly working capillary barrier. Our experimental results and data analyses indicate that prediction of capillary barrier performance based on standard hydraulic property parameter measurements and the Richards' equation is not always adequate for predicting detailed system behavior.

The (Tempe cell) measured hydraulic parameters were very similar in both experiments but produced different observed results. To explain the observed differences, we measured the surface profiles and roughness of the two sands and conducted an additional vapor diffusion experiment. Based on theoretical calculations and the vapor diffusion experiments, the primary controlling mechanism in this system appears to be the magnitude of the surface area and the roughness of the materials, resulting in varying rates of infiltration due to differing film flow infiltration velocities.

Typical hydrologic modeling of unsaturated flow based on Richards' equation generally excludes dry regime flow processes, which can have significant impacts on flow and transport in dry systems in semiarid and arid climates. Our numerical simulations showed how pseudo-film flow was a possible method for

simulating the barrier failure observed in the experiments as well as the observed differences between the two experiments. Thus, we conclude that for experiments conducted at low saturation, considering material characteristics (such as surface area and roughness) in addition to traditional hydraulic properties may be necessary to fully describe the system behavior. We believe this is especially important to consider when dealing with capillary barrier design. Future numerical models could be improved by extending the hydraulic conductivity–saturation functions to mimic water film infiltration velocities as a function of surface roughness.

Despite the fact that water infiltrated the lower coarse material in both of our experiments, it is notable that the majority of the water was diverted by the drains in both cases (93.3% for the angular sand and 99.7% for the round sand). It is also important to consider that the irrigation pattern and amounts applied here would not necessarily occur in natural systems, which could have an impact on a capillary barrier's long-term performance. Additional testing of the capillary barrier system under multiple irrigation scenarios would be required to fully characterize system performance.

Acknowledgments

This work was performed under the auspices of the U. S. Department of Energy (DOE) by the University of California, Lawrence Livermore National Laboratory, under Contract no. W-7405-Eng-48 and was funded by the DOE. Additional funding was provided by Oregon State University Subsurface Biosphere NSF IGERT program and Oregon State University, Institute for Water and Watersheds Graduate Student Research Grant. Special thanks to Gaurav Saini for his assistance with obtaining surface profiles of the sands, and to Ida L. Fabricius, Dep. of Environmental Engineering, Danish Technical University, for help with acquisition and interpretation of the BET data.

References

Aminzadeh, B., and D.A. DiCarlo. 2010. The transition between sharp and diffusive wetting fronts as a function of imbibing fluid properties. Vadose Zone J. 9:588–596. doi:10.2136/vzj2009.0072

Bear, J. 1988. Dynamics of fluids in porous media. Dover Publ., New York.

Bico, J., U. Thiele, and D. Quéré. 2002. Wetting of textured surfaces. Colloids Surf. A 206:41–46. doi:10.1016/S0927-7757(02)00061-4

Bico, J., C. Tordeux, and D. Quéré. 2001. Rough wetting. Europhys. Lett. 55:214–220. doi:10.1209/epl/i2001-00402-x

Brooks, R.H., and A.T. Corey. 1964. Hydraulic properties of porous media. Hydrol. Pap. 3. Colorado State Univ., Fort Collins, CO.

Brunauer, S., P.H. Emmett, and E. Teller. 1938. Adsorption of gases in multimolecular layers. J. Am. Chem. Soc. 60:309–319. doi:10.1021/ja01269a023

Cass, A., G.S. Campbell, and T.L. Jones. 1984. Enhancement of thermal water vapor diffusion in soil. Soil Sci. Soc. Am. J. 48:25–32. doi:10.2136/sssaj1984.03615995004800010005x

Conca, J.L. 1990. Diffusion barrier transport properties of unsaturated paintbrush tuff rubble backfill. p. 394–401. In Proc. Int. High-Level Radioactive Waste Management Conf., 1st, Las Vegas, NV. 28 Apr.–3 May 1990. Am. Nucl. Soc., La Grange Park, IL.

Derjaguin, B.V., and N.V. Churaf. 1976. Polymolecular adsorption and capillary condensation in narrow slit pores. J. Colloid Interface Sci. 54:157–174. doi:10.1016/0021-9797(76)90298-8

DiCarlo, D.A., T.W.J. Bauters, C.J.G. Darnault, T.S. Steenhuis, and J.-Y. Parlange. 1999. Lateral expansion of preferential flow paths in sands. Water Resour. Res. 35:427–434. doi:10.1029/1998WR900061

Dullien, F. 1992. Porous media: Fluid transport and pore structure. Academic Press, New York.

Easton, E.B., and W.D. Machin. 2000. Adsorption of water vapor on a graphitized carbon black. J. Colloid Interface Sci. 231:204–206. doi:10.1006/jcis.2000.7116

Hay, K.M., M.I. Dragila, and J. Liburdy. 2008. Theoretical model for the wetting of a rough surface. J. Colloid Interface Sci. 325:472–477. doi:10.1016/j.jcis.2008.06.004

Ho, C.K., and S.W. Webb. 1998. Enhanced vapor-phase diffusion in porous media. LDRD Final Rep. Sandia National Lab., Albuquerque, NM.

Hu, Q., T. Kneafsey, J.J. Roberts, L. Tomutsa, and J.S.Y. Wang. 2004. Characterizing unsaturated diffusion in porous tuff gravel. Vadose Zone J. 3:1425–1438.

Ishino, C., K. Okumura, and D. Quéré. 2004. Wetting transitions on rough surfaces. Europhys. Lett. 68:419–425. doi:10.1209/epl/i2004-10206-6

Jabro, J.D. 2009. Water vapor diffusion through soil as affected by temperature and aggregate size. Transp. Porous Media 77:417–428. doi:10.1007/s11242-008-9267-z

Klute, A. (ed.) 1986. Methods of soil analysis. Part 1. 2nd ed. Agron. Monogr. 9. ASA and SSSA, Madison, WI.

Kutilek, M., and D.R. Nielsen. 1994. Soil hydrology. Catena-Verlag, Reiskirchen, Germany.

Martines, E., K. Seunarine, H. Morgan, N. Gadegaard, C.D.W. Wilkinson, and M.O. Riehle. 2005. Superhydrophobicity and superhydrophilicity of regular nanopatterns. Nano Lett. 5:2097–2103. doi:10.1021/nl051435t

Mualem, Y. 1976. New model for predicting hydraulic conductivity of unsaturated porous media. Water Resour. Res. 12:513–522. doi:10.1029/WR012i003p00513

Nimmo, J.R. 1991. Comment on the treatment of residual water content in "A consistent set of parametric models for the two-phase flow of immiscible fluids in the subsurface" by L. Luckner et al. Water Resour. Res. 27:661–662. doi:10.1029/91WR00165

Nimmo, J.R., D.A. Stonestrom, and K.A. Akstin. 1994. The feasibility of recharge rate determinations using the steady-state centrifuge method. Soil Sci. Soc. Am. J. 58:49–56. doi:10.2136/sssaj1994.03615995005800010007x

Nitao, J.J. 1998. Reference manual for the NUFT flow and transport code, version 2.0. Lawrence Livermore National Lab., Livermore, CA.

Nitao, J.J., and J. Bear. 1996. Potentials and their role in transport in porous media. Water Resour. Res. 32:225–250. doi:10.1029/95WR02715

Parker, J. 1986. Hydrostatics of water in porous media. CRC Press, Boca Raton, FL.

Quéré, D. 2002. Rough ideas on wetting. Physica A 313:32–46.

Quéré, D. 2008. Wetting and roughness. Annu. Rev. Mater. Res. 38:71–99. doi:10.1146/annurev.matsci.38.060407.132434

Quéré, D., and J. Bico. 2003. Controlled wetting by surface patterning. Houille Blanche 2003(4):21–24.

Rossi, C., and J.R. Nimmo. 1994. Modeling of soil water retention from saturation to oven dryness. Water Resour. Res. 30:701–708. doi:10.1029/93WR03238

Tidwell, V.C., R.J. Glass, C. Chocas, G. Barker, and L. Orear. 2003. Visualization experiment to investigate capillary barrier performance in the context of a Yucca Mountain emplacement drift. J. Contam. Hydrol. 62–33:287–301. doi:10.1016/S0169-7722(02)00164-X

Tokunaga, T.K. 1997. A tensiometer for measuring hydraulic potentials on surfaces of porous rock. Water Resour. Res. 33:1509–1513. doi:10.1029/97WR00474

Tokunaga, T.K., and J.M. Wan. 1997. Water film flow along fracture surfaces of porous rock. Water Resour. Res. 33:1287–1295. doi:10.1029/97WR00473

Tokunaga, T.K., and J.M. Wan. 2001. Approximate boundaries between different flow regimes in fractured rocks. Water Resour. Res. 37:2103–2111. doi:10.1029/2001WR000245

Tokunaga, T.K., J.M. Wan, and S.R. Sutton. 2000. Transient film flow on rough fracture surfaces. Water Resour. Res. 36:1737–1746. doi:10.1029/2000WR900079

Tuller, M., and D. Or. 2001. Hydraulic conductivity of variably saturated porous media: Film and corner flow in angular pore space. Water Resour. Res. 37:1257–1276. doi:10.1029/2000WR900328

Tuller, M., D. Or, and L.M. Dudley. 1999. Adsorption and capillary condensation in porous media: Liquid retention and interfacial configurations in angular pores. Water Resour. Res. 35:1949–1964. doi:10.1029/1999WR900098

Tzevelekos, K.P., E.S. Kikkinides, M.E. Kainourgiakis, A.K. Stubos, N.K. Kanellopoulos, and V. Kaselouri. 2000. Adsorption–desorption flow of condensable vapors through mesoporous media: Network modeling and percolation theory. J. Colloid Interface Sci. 223:89–101. doi:10.1006/jcis.1999.6659

van Genuchten, M.Th. 1980. A closed-form equation for predicting the hydraulic conductivity of unsaturated soils. Soil Sci. Soc. Am. J. 49:1354–1359.

Webb, S.W. 1997. Generalization of Ross' tilted capillary barrier diversion formula for different two-phase characteristic curves. Water Resour. Res. 33:1855–1859. doi:10.1029/97WR01231

Wenzel, R.N. 1936. Resistance of solid surfaces to wetting by water. Ind. Eng. Chem. 28:988–994. doi:10.1021/ie50320a024

Wildenschild, D., K.H. Jensen, K.J. Hollenbeck, T. Sonnenborg, M.B. Butts, T.H. Illangasekare, and D. Znidarcic. 1997. A two-stage procedure for determining unsaturated hydraulic characteristics using a syringe pump and outflow observations. Soil Sci. Soc. Am. J. 61:347–359. doi:10.2136/sssaj1997.03615995006100020002x

Wildenschild, D., and J.J. Roberts. 2001. Experimental tests of enhancement of vapor diffusion in Topopah Spring tuff. J. Porous Media 4:1–13.